Correlation between the bath composition and nanoporosity of DC-electrodeposited Ni-Fe alloy

Correlation between the Bath Composition and Nanoporosity of DC-Electrodeposited Ni-Fe Alloy

Journal:	*Surface and Interface Analysis*
Manuscript ID	Draft
Wiley - Manuscript type:	ECASIA special issue paper
Date Submitted by the Author:	n/a
Complete List of Authors:	Maizza, Giovanni; Politecnico di Torino, DISAT pero, renato; University of Rome Tor Vergata, industrial engineering Kaciulis, Saulius; CNR, ISMN Bolli, Eleonora; CNR, ISMN; University of Rome Tor Vergata, industrial engineering Eom, Hyeonjin; Korea Institute of Industrial Technology, Thermochemical Energy R&D Group Lee, Minsu; Hanyang University, Department of Materials Science and Engineering; Korea Institute of Industrial Technology, Surface Technology R&D Group Yim, Tai; Korea Institute of Industrial Technology, Surface Technology R&D Group
Keywords:	XPS, Ni-Fe alloy, Corncob structure, Nanocrystalline films, Nanoporosity, Electrodeposition

Correlation between the Bath Composition and Nanoporosity of DC-Electrodeposited Ni-Fe Alloy

G. Maizza[1]*, R. Pero[2], S. Kaciulis[3], E. Bolli[3], H. Eom[4], M. Lee[5,6] and T.H. Yim[6]

1 Department of Applied Science and Technology, Politecnico di Torino, Torino, 10129, Italy

2 Department of Industrial Engineering, University of Rome "Tor Vergata", Roma, 00133, Italy

3 Institute for the Study of Nanostructured Materials, ISMN — CNR, Monterotondo Stazione, Rome 00015, Italy

4 Thermochemical Energy R&D Group, Korea Institute of Industrial Technology, Seobuk-gu, Cheonan-si, 31056, Republic of Korea

5 Department of Materials Science and Engineering, Hanyang University, Seoul, 04763, Republic of Korea

6 Surface Technology R&D Group, Korea Institute of Industrial Technology, Yeonsu-gu, Incheon 21999, Republic of Korea

***corresponding author:** maizza@polito.it

ORCID Identifiers

G. Maizza: orcid.org/0000-0002-1374-4418

R. Pero: orcid.org/0000-0002-8944-565X

S. Kaciulis: orcid.org/0000-0002-9868-7626

E. Bolli: https://orcid.org/0000-0002-6079-0900

H. Eom: orcid.org/0000-0003-3423-4334

M. Lee: orcid.org/0000-0002-0510-1105

T.H. Yim: orcid.org/0000-0002-5570-3411

Abstract

The outstanding mechanical strength of as-deposited DC-electrodeposited nanocrystalline (nc) Ni-Fe alloys has been the subject of numerous researches in view of their scientific and practical interest. However, recent studies have reported a dramatic drop in ductility upon annealing above 350 °C, associated with a concomitant abnormal rapid grain growth. The inherent cause has been ascribed to the presence of a detrimental product or by product in the bath which affects either the microstructure or causes defects in the concentration and/or distribution of the as-deposited films. The present work has been inspired by the observed abnormal behaviour of annealed electrodeposited nc Ni-Fe alloy, which has here been addressed by considering the relationship between the composition of the bath (iron-chloride, nickel-sulphate solution, saccharin and ascorbic acid) and deposition defects (e.g., grain boundary pores) in the case of an nc Ni-Fe (Fe 48wt%) alloy. The current investigations have included X-ray photoelectron spectroscopy (XPS), field emission scanning electron microscopy (FESEM) and transmission electron microscopy (TEM) in both as-deposited and post-annealed conditions (300–400 °C). XPS depth profiling with Ar ion sputtering showed a significant amount of C and O impurities entrapped in the foils during deposition. As such impurities are often overlooked in common analytical techniques, new scenarios may need to be rationalised to explain the observed drop in tensile ductility of the as-deposited Ni-Fe alloys.

Keywords: XPS, Ni-Fe alloy, Corncob structure, Electrodeposition, Thin films, Nanocrystalline films, Nanoporosity

Introduction

Electrodeposition is a viable and low-cost manufacturing technology of nanocrystalline (nc) thin films and free-standing foils of controlled composition, purity, grain size and thickness [1]. The potential applications of nc Ni-Fe alloys range from micro-electro-mechanical systems to solar cells, organic light-emitting diodes, magnetic devices and functional coatings, in force of their unique magnetic, thermal and mechanical properties [2] [3] [4] [5] [6] [7] [8] [9]. Despite the versatility of the electrodeposition process, in terms of alloy types, chemical compositions, microstructure and properties [1], process control is difficult as a result of such factors as the bath composition, current density, pH and temperature. The fabrication of nc Ni-Fe alloys by means of the DC-electrodeposition process, in its simplest form, utilises a constant current density (*j*) [1]. Most researches have dealt with the relationship between the chemical composition, grain size, magnetic properties and thermal properties (see, for instance, refs. [1] [10] [7] [11] [12]). As far as the bath composition is concerned, it has been reported that a sulphamate bath promotes a high deposition rate and minimal internal stresses [1].The addition of saccharin acts as a grain refiner and stress reliever [1] [12] [13] [14] [15] [16]. Both boric acid and ascorbic acid reduce hydroxide deposition on the alloy surface [1]. Moreover, while the former expands the current density window of the process [1] and increases the oxygen content dissolved in the deposit [17], the latter prevents the oxidation of Fe^{2+}/Fe^{3+} during the process [1]. On the other hand, chemical additives in the bath markedly influence the final composition of the foils [18] [19] [20]. An increased content of saccharin has been found to lead to an increased amount of entrapped S and C in the deposits [18]. The excess of S in a sulphamate bath has been correlated to a rapid drop in

ductility [19], but has shown a negligible influence on solid solution strengthening [20]. The increase in hardness, due to interstitial C, has been confirmed in the case of Ni electrodeposits [19].

FESEM studies over the cross-section of a chemically etched as-deposited Ni-48 wt% Fe foil have revealed the presence of a network of sub-micrometer pores, mostly at the boundaries of columnar grains [21], which are believed to be partly (if not dominantly) caused by bath impurities. Most of such pores were found to be distributed along columnar grain boundaries and they act as weakeners of intergranular bonds. Such weak grain boundaries often culminate in mode-I fracturing in conventional tensile tests. As a result, the foils of these types suffer from extremely low ductility and excessive brittleness. Only a few studies have addressed the correlation between the composition of the bath and the grain size of the foils and/or that of the Ni/Fe ratio [1]. However, to the best of the authors' knowledge, no studies have addressed the relationship between bath contaminants (except Sulphur) and their potential entrapment in nc Ni-Fe electrodeposits.

Thus, it has been the aim of this study to cross-link TEM and FESEM inspections along with chemical analysis, such as XPS and ICP-MS, to search for a possible correlation between bath additives and detrimental impurities, which are commonly observed at the columnar grain boundaries, and are considered to be responsible for the low tensile ductility of as-deposited and annealed Ni-49 at% Fe alloy foils.

Materials and methods

An electrolytic bath (pH 3.5 and 55 °C), containing iron (II) chloride 0.1 M, nickel (II) sulphamate 0.6 M, boric acid 0.5 M, ascorbic acid 0.005 M and saccharin 0.05 M, has been considered. The cathode and the anode electrodes consisted of 130 x 130 mm^2 plates made of AISI 304 stainless steel (super mirror-finish) and Ni. A sketch of the DC-electrodeposition process is shown in Fig. 1. The deposition process was conducted under a DC condition (60 mA cm^{-2}). First, nc Ni-49 at% Fe alloy films were deposited over the cathode surface at thicknesses of up to 200 ± 10 µm and then mechanically stripped as free-standing foils [9]. Subsequently, the as-deposited foils were annealed in an H_2+N_2 gas atmosphere at 320, 350 and 370 °C at a 5 °C/min heating rate, and this was followed by a 60 min holding time to thermally stabilise the nc alloys.

The top surface of the as-deposited samples was examined by means of high-resolution field emission scanning electron microscopy (FESEM) and energy dispersive X-ray spectroscopy (EDS), while their cross-sections were analysed using transmission electron microscopy (TEM).

The chemical surface analysis and depth profiling of the as-deposited and annealed foils were executed by X-ray photoelectron spectroscopy (XPS) in an Escalab MkII spectrometer (VG Scientific Ltd, UK) using an Al Kα source and cyclic Ar^+ sputtering with a rastered EX-05 ion gun kept at an energy level of 2.0 keV, which corresponds to a sputtering rate of 0.25 nm/min. Quantitative information on the Ni and Fe contents was obtained from the Fe 3p and Ni 3p spectra, as the main Fe 2p peak of iron overlaps the Ni LMM Auger signal, and their separation is very difficult. The binding energy (BE) scale was calibrated by positioning the C 1s peak of adventitious carbon at BE = 285.0 eV. All the experimental data were acquired and processed by Avantage v.5 software (Thermo Fisher Scientific Ltd, UK).

The presence of bath impurities in the as-deposited foils was assessed using inductive coupled plasma mass spectroscopy (ICP-MS, NexION 350D, Perkin Elmer) with 0.3–3.0 amu resolution in Ar-plasma (6000 K) and a 1.00 ml min^{-1} sample injection flow rate.

Results

The high resolution FESEM revealed that the columnar structure of the DC-electrodeposited Ni-Fe foils resembled that of a *corncob* [21] with a *nested three-scale hierarchy* polycrystalline structure, ranging from the nanoscopic scale (~ 10 nm) to the sub-micron scale (up to 250 nm), across a mesoscopic scale (155-165 nm). The present TEM results pertaining to a cross-section view (Fig. 2.a) and the FESEM results referring to the top view (Fig. 2.b) of the as-deposited foils have confirmed a columnar grain structure (dashed lines) and the presence of impurity segregations and/or that of pores at their grain boundaries. The EDS spectra over the top surface in both the as-deposited (Fig. 3.a) and 370 °C annealed (Fig. 3.b) samples detected a constant atomic Ni to Fe ratio of 1. As previous results of XPS analysis indicated an identical chemical composition at the top and bottom surfaces of the as-deposited foils, other XPS depth profiling investigations were executed, albeit only on the top surface. The obtained results showed the presence of C and O as the main contaminant species (apart from Ni and Fe) and traces of Sn (Fig. 4.a). XPS probing of other zones on the sample surface (not shown) also revealed the occasional presence of S (up to 3 at%) and Ca (up to 1.5 at%). The amount of impurities in the Ni-49 at% Fe alloy markedly decreased at a sputtering depth of about 5 nm, as shown in Figs. 4.a and 5.a. The latter figure depicts the ratio of the impurity/(Ni+Fe) vs. sputtering depth.

The XPS depth profiling of the annealed samples evidenced analogous results, namely, significant amounts of C and O on the sample surface (Fig. 4.b, 4.c and 4.d), and a decrease in the impurity content at a sputtering depth of about 5 nm (Fig. 5.a). Some traces of S and Sn were observed in the sample annealed at 370 °C (Fig. 4.c). The XPS depth profile of the sample annealed at 320 °C is shown in Fig G, where the scale of the normalised peak area vs. sputtering depth is used. The use of the normalised area (Fig. 6) rather than the atomic concentration (Fig. 4) helps to univocally understand any possible relationship between the variation in the elemental signals with the sputtering depth.

Fig. 5b shows the Ni/Fe atomic ratio as a function of the sputtering depth for the as-deposited and the annealed foils after XPS. The Ni/Fe ratio markedly deviates from the nominal value (dashed line), depending on the sputtering depth and annealing temperature.

Inductively coupled plasma mass spectroscopy (ICP-MS) confirmed, among others (Table 1), the presence of 4.53 10^5 ppb of Ca and 1.9 10^3 ppb of Sn in the as-deposited foil, whereas previous investigations [21] of analogous as-deposited alloy, using inductively coupled plasma atomic emission spectroscopy (ICP-OES), revealed 409.41 ppm of S.

Discussion

The current efficiency (CE) of the DC-electrodeposition process is usually very close to 100 %, and it is defined as the ratio between the weight of the actual deposited metal and that predicted by Faraday's law (w_{th}) [22]:

$$w_{th} = \frac{A_{wt}\, j\, A_{an}\, t}{n\, F} \qquad \text{Eq. 1}$$

where A_{wt} is the average atomic weight of the electrodeposited species, j is the current density, A_{an} is the anode area, t is the deposition time, n is the number of electrons involved in the deposition reaction (equal to 2 in the case of Ni and Fe) and F is Faraday's constant (96487 C mol^{-1}). Assuming an atomic Ni/Fe ratio of 1, the average atomic weight of the investigated alloy is 57.26 g mol^{-1} which, for a 100 min deposition time, gives 18.05 g. As the measured weight of the actual foils is 17.04 g, the current efficiency (CE) of the process is as high as 94%.

The EDS analysis gave an atomic ratio of Ni/Fe of 1.2, which compares well with 1.03 nominal ratio. Moreover, such a ratio remains constant after an annealing treatment. On the other hand, the XPS depth profile shows (Fig. 5.b) that it changes noticeably according to the etched depth and the annealing temperature and that it may locally be either much larger or much lower than the nominal value. This suggests that, unlike the micro-scale (EDS analysis), the Ni/Fe ratio is not homogeneous over a local nano-scale (XPS). In addition, the XPS results revealed that the O content (very significant on the surface) is composed of two different species. The first one at BE, in the $532 - 534$ eV range, registered on the non-sputtered surface, is associated with –OH, H_2O, CO and C=O groups, and it has therefore been denoted as adsorbed O. The second one, which is the major contributor after ion sputtering, has a BE of about 530 eV, which is typical of Ni and Fe oxides, and it has therefore been denoted as oxide O. These results can be compared with other works, based on EDS analysis [10]which, in analogous electrodeposited Ni-Fe alloys (7–31.55 wt% Fe), approximately gave values of up to 0.6 at.% (27 wt.%) of O, which were ascribed to the concurrent deposition of pure metallic ions and their oxides. In the same reference [10], the authors found that the O content increased with a decreasing Ni/Fe ratio. That evidence supports the high O content observed here in the Ni-49 at% Fe alloy.

The XPS depth profiles in Fig. 4 show that a decrease in the O content corresponds to an increase in the Ni+Fe content. In general, the drop in O is linked with a decrease in C, although there are some exceptions. For example, in the as-deposited sample in Fig. 4.a, the gradient of the C concentration is in fact higher than that of O. Furthermore, the annealed sample at 320 °C (Fig. Bb) exhibits an increase in C at a sputtering depth of 4 nm but does not show any increase in the O content. This suggests that the profiles of C and O vs. depth are unrelated. At a first glance, the reduction in the O and C contents is linked to the increase in Ni and Fe. However, an inspection of the depth profiles of the as-deposited sample and those of the 320 and 350 °C annealed samples (orange circles in Figs. 4.a, 4.b and 4.c) suggests that a decrease in the C content corresponds to an increase in Ni, and vice versa, regardless of the presence of Fe. This implies that C may replace Ni in the Ni-Fe solid solution to some extent. Figure 6 confirms the results depicted in Fig. 4.b in that the at% of Ni and C inside the dashed circle are intimately correlated. A relevant amount of C, as shown in this study, was also found at the fracture surface of an electroplated 80Ni-20Fe

Permalloy by means of Auger depth profiling measurements [23]. The Auger depth profile in Fig. 5.b of ref. [23] shows a similar relationship between C and Ni to that shown in Figs. 4.a, 4.b, 4.c and 6 (orange circles), although the authors ascribed the detected C to an "artificial contamination".

Previous investigations carried out by one of the authors (S.K.) revealed that graphitic and/or amorphous C may be incorporated in a metallic alloy by substitutionally (rather than interstitially) replacing one of the constituent metals [24]. This phenomenon may also have occurred here in the case of Ni and C. It should be noted that the C 1s signal with BE = 284.6 eV corresponds to graphitic and/or amorphous carbon boundaries and enters the Ni-Fe solid solution as a substitutional rather than an interstitial foreign element. Only the excessive C content (aliphatic with BE = 285.0 eV), detected on the non-sputtered surface, may be due to a post-process ambient contamination of the foil. In principle, the C present in the subsurface may either have diffused from the surface or been trapped in the film during deposition. Broadly speaking, the monotonic C profile in Figure 4.a may be explained as a simple diffusion process from the surface, driven by a carbon source available on the surface. However, the irregular profiles of C shown in Figs. 4.b and 4.d indicate that this is actually unlikely, and that the bath and the associated deposition process are more likely its origin, as clearly supported by the intimate link between C and Ni profiles in the bulk in Figs. 4.a, 4.b and 4.c.

Sulphur has been considered as a polluting element in both electrodeposited pure Ni [25] [26] [27] and Ni-Fe alloys [19] [23] [28] [29] originating from saccharin in the bath. It is likely to be trapped in the film during deposition. Its detrimental role on the elongation-to-fracture has been reported by various authors [19] [23] [26]. Sulphur was found to be approximately 0.07 at% (or 409.41 ppm) (by ICP-OES analysis) in an Ni-49 at% Fe alloy [21], in agreement with other studies and similar Ni-Fe alloys [19] [29]. However, such a low content of Sulphur cannot be accurately appreciated by means of EDS measurements. In this work, the XPS analysis occasionally detected Sulphur at some points on the surface in both the as-deposited and annealed samples (Fig. 4). Its distribution over the foil surface should be considered as inhomogeneous and preferentially located at the pores along the columnar grain boundaries (Figs. 2.a and 2.b).

Conclusions

An investigation on the relationship between bath composition (iron-chloride, nickel-sulphate solution, saccharin and ascorbic acid) and deposition defects (*e.g.*, grain boundary pores) in electrodeposited nc Ni-Fe (Fe 48wt%) alloy has been undertaken in order to explain the observed poor elongation-to-fracture and abnormal fracture behaviour of electrodeposited nc Ni-Fe alloy under annealed conditions.

Quantitative chemical analysis, conducted on Ni-49 at% Fe alloy foils, has revealed that C, O and S are the main impurities preferentially located at the columnar grain boundaries.

The non-monotonic XPS depth profile of C (320 and 370 °C annealed samples) suggests that the C was trapped, during the deposition process, from organic additives, whereas S originated from saccharin.

The XPS depth profiles revealed a close relationship between C and Ni, thus indicating a possible substitutional replacement, to some extent, of Ni by C in the Ni-Fe solid solution.

XPS detected two possible origins of Oxygen species: a) from adsorbed species on the film surface, where it is copiously present, b) at the sub-surface region, in a lower amount, as Ni and Fe oxides formed as side-effects during the Ni-Fe co-deposition process.

The XPS results indicate that the Ni/Fe ratio is inhomogeneously distributed over a nano-scale (and is undetectable by means of micro-scale EDS) and depends to a great extent on the annealing temperature.

References

[1] Torabinejad V, Aliofkhazraei M, Assareh S, Allahyarzadeh MH, Rouhaghdam AS. Electrodeposition of Ni-Fe alloys, composites, and nano coatings–A review. J Alloy Compd 2017;691:841-859.

[2] Mazza E, Abel S, Dual J. Experimental determination of mechanical properties of Ni and Ni-Fe microbars. Microsystem Technologies 1996;2(4):197-202

[3] Kurmanaeva L, McCrea J, Jian J, Fiebig J, Wang H, Mukherjee AK, Lavernia EJ. Influence of layer thickness on mechanical properties of multilayered NiFe samples processed by electrodeposition. Materials Design 2016;90:389-395.

[4] Torabinejad V, Aliofkhazraei M, Rouhaghdam AS, Allahyarzadeh MH. Functionally graded coating of Ni-Fe fabricated by pulse electrodeposition. J of Mater Eng Perform 2016;25(12):5494-5501.

[5] Hibbard GD, Erb U, Aust KT, Klement U, Palumbo G. Thermal stability of nanostructured electrodeposits. Mater Sci Forum 2002;386:387-396.

[6] McCrea JL, Palumbo G, Hibbard GD, Erb U. Properties and applications for electrodeposited nanocrystalline Fe-Ni alloys. Reviews on Adv Mater Sci 2003;5(3):252-258.

[7] Tabakovic I, Inturi V, Thurn J, Kief M. Properties of Ni1− xFex (0.1< x< 0.9) and Invar (x= 0.64) alloys obtained by electrodeposition. Electrochimi Acta 2010;55(22):6749-6754.

[8] Nagayama T, Yamamoto T, Nakamura T. Thermal expansions and mechanical properties of electrodeposited Fe–Ni alloys in the Invar composition range. Electrochimi Acta 2016;205:178-187.

[9] Lee M, Ahn J, Yim TH. Effects of Electroformed Fe-Ni Substrate Textures on Light-trapping in Thin Film Solar Cells. Int J Electrochem Sci 2018;13:5612-5619.

[10] Abdel-Karim R, Reda Y, Muhammed M, El-Raghy S, Shoeib M, Ahmed H. Electrodeposition and characterization of nanocrystalline Ni-Fe alloys. J Nanomaterials 2011;2011:7.

[11] Chang WS, Wei Y, Guo JM, He FJ. Thermal stability of Ni-Fe alloy foils continuously electrodeposited in a fluorborate bath. Open J met 2012;2(01):18.

[12] Kim SH, Sohn HJ, Joo YC, Kim YW, Yim TH, Lee HY, Kang T. Effect of saccharin addition on the microstructure of electrodeposited Fe–36 wt.% Ni alloy. Surf Coat Tech 2005;199(1):43-48.

[13] Zhang YH, Ding GF, Cai YL, Wang H, Cai B. Electroplating of low stress permalloy for MEMS. Mater charact 2006;57(2):121-126.

[14] Bhandari A, Hearne SJ, Sheldon BW, Soni SK. Microstructural origins of saccharin-induced stress reduction in electrodeposited Ni. J Electrochem Soc 2009;156(8):D279-D282.

[15] Kim SH, Sohn HJ, Joo YC, Kim YW, Yim TH, Lee HY, Kang T. Effect of saccharin addition on the microstructure of electrodeposited Fe–36 wt.% Ni alloy. Surf Coat Tech 2005;199(1):43-48

[16] Chaudhari AK, Singh VB. A review of fundamental aspects, characterization and applications of electrodeposited nanocrystalline iron group metals, Ni-Fe alloy and oxide ceramics reinforced nanocomposite coatings. J Alloy Comp 2018;751:194-214.

[17] Gadad S, Harris TM. Oxygen Incorporation during the Electrodeposition of Ni, Fe, and Ni-Fe Alloys. J Electrochem Soc 1998;145(11):3699-3703.

[18] El-Sherik AM, Erb U. Synthesis of bulk nanocrystalline nickel by pulsed electrodeposition. J Mater Sci 1995;30(22):5743-5749.

[19] Li H, Jiang F, Ni S, Li L, Sha G, Liao X, Ringer SP, Choo H, Liaw P, Misra A. Mechanical behaviors of as-deposited and annealed nanostructured Ni–Fe alloys. Scr Mater 2011;65(1):1-4.

[20] Matsui I, Uesugi T, Takigawa Y, Higashi K. Effect of interstitial carbon on the mechanical properties of electrodeposited bulk nanocrystalline Ni. Acta Mater 2013;61(9):3360-3369.

[21] Maizza G, Eom H, Lee M, Yim TH, Nakagawa E, Pero R, Ohmura T. Mechanical and fracture behaviour of the three-scale hierarchy structure in As-deposited and annealed nanocrystalline electrodeposited Ni–Fe alloys. J Mater Sci 2019;54(20):13378-13393.

[22] Schlesinger M, Paunovic M. Modern electroplating. Hoboken, New Jersey: John Wiley & Sons. 2011. 7p.

[23] Buchheit TE, Goods SH, Kotula PG, Hlava PF. Electrodeposited 80Ni–20Fe (Permalloy) as a structural material for high aspect ratio microfabrication. Mater Sci Eng A 2006;432(1-2):149-157.

[24] Ciancaglioni I, Donnini R, Kaciulis S, Mezzi A, Montanari R, Ucciardello N, Verona-Rinati G. Surface modification of austenitic steels by low-temperature carburization. Surf Int Anal 2012;44(8);1001-1004.

[25] Kolonits T, Jenei P, Tóth BG, Czigány Z, Gubicza J, Péter L, Bakonyi I. Characterization of defect structure in electrodeposited nanocrystalline Ni films. J Electrochem Soc 2016;163(3):D107-D114.

[26] Matsui I, Ohte R, Omura N, Takigawa Y. Thermal embrittlement and microstructure change in electrodeposited Ni. Mater Sci Eng A 2019;745:168-175.

[27] Abraham M, Holdway P, Thuvander M, Cerezo A, Smith GDW. Thermal stability of electrodeposited nanocrystalline nickel. Surf Eng 2002;18(2):151-156.

[28] Kouncheva M, Raichevski G, Prazak M The effect of sulphur and carbon inclusions on the corrosion resistance of electrodeposited Ni-Fe alloy coatings. Surf Coat Tech 1987;31(2):137-142.

[29] Mori H, Matsui I, Takigawa Y, Uesugi T, Higashi K. Reduction in sulfur content of electrodeposited bulk nanocrystalline Fe–Ni alloys using manganese chloride. Mater Lett 2016;175:86-88.

Table 1: ICP-MS results of the as-deposited Ni-49 at% Fe foils

Element	Amount (ppb)	Element	Amount (ppb)	Element	Amount (ppb)
Ca	45354	Mn	7994	Pb	21369
Cr	347	Co	519540	Sn	1927
As	3995224	Cu	50301	Ge	62439
Al	4627	Zn	21663017	Mo	61783
K	10014	Ru	2168	-	-

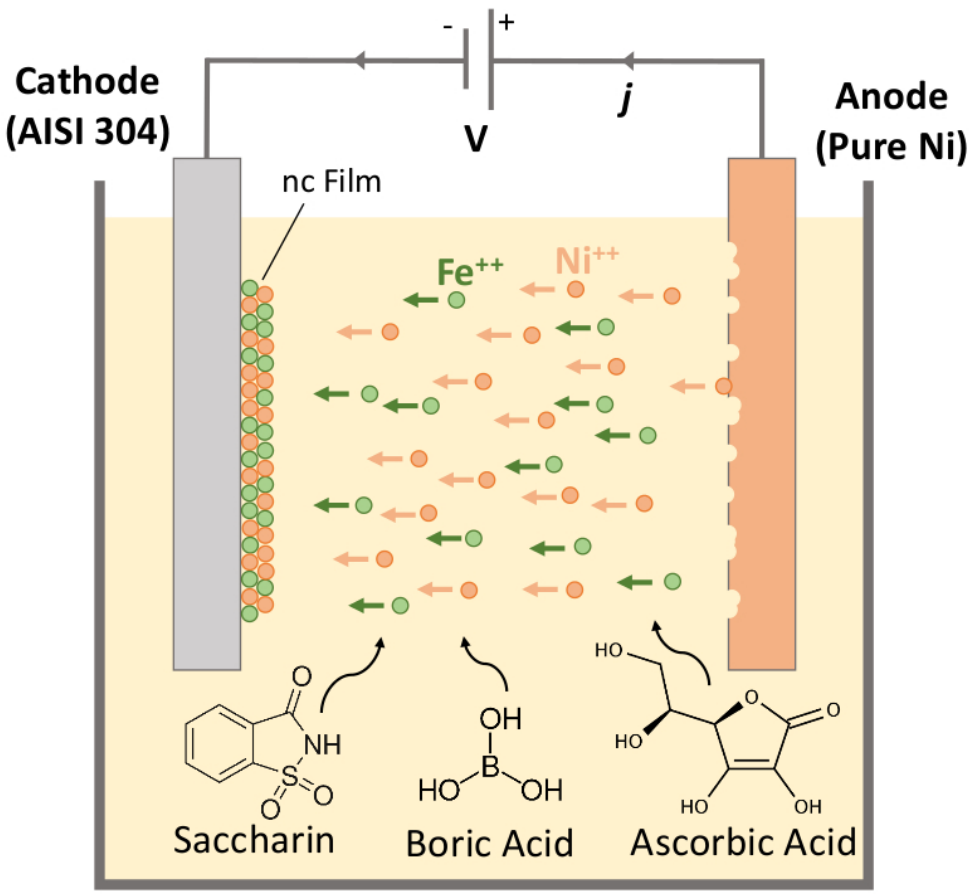

Figure 1: Sketch of the DC-electrodeposition process of the nanocrystalline Ni-49 at% Fe alloy.

201x184mm (100 x 100 DPI)

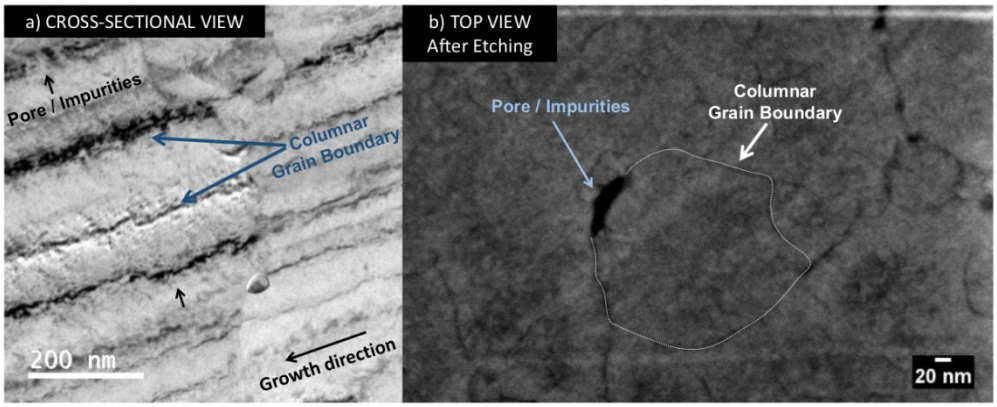

Figure 2: a) TEM image: cross-sectional of the nc Ni-Fe foil; b) high magnification FESEM image of the top view surface after selective etching of the as-deposited sample

316x128mm (100 x 100 DPI)

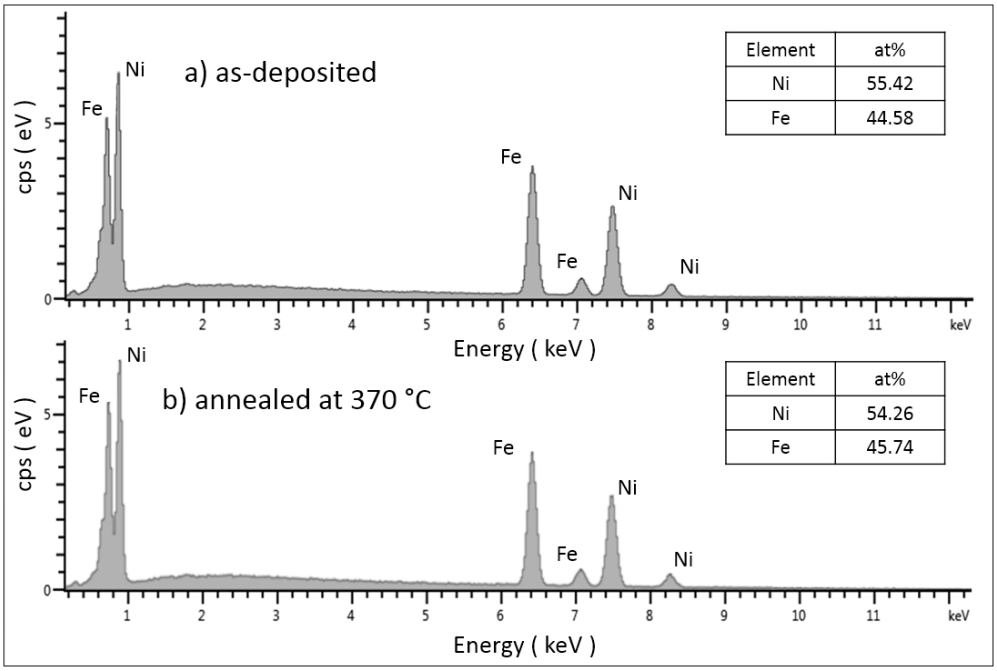

Figure 3: EDS analysis on the top view surface: a) as-deposited sample; b) annealed samples at 370 °C

279x187mm (100 x 100 DPI)

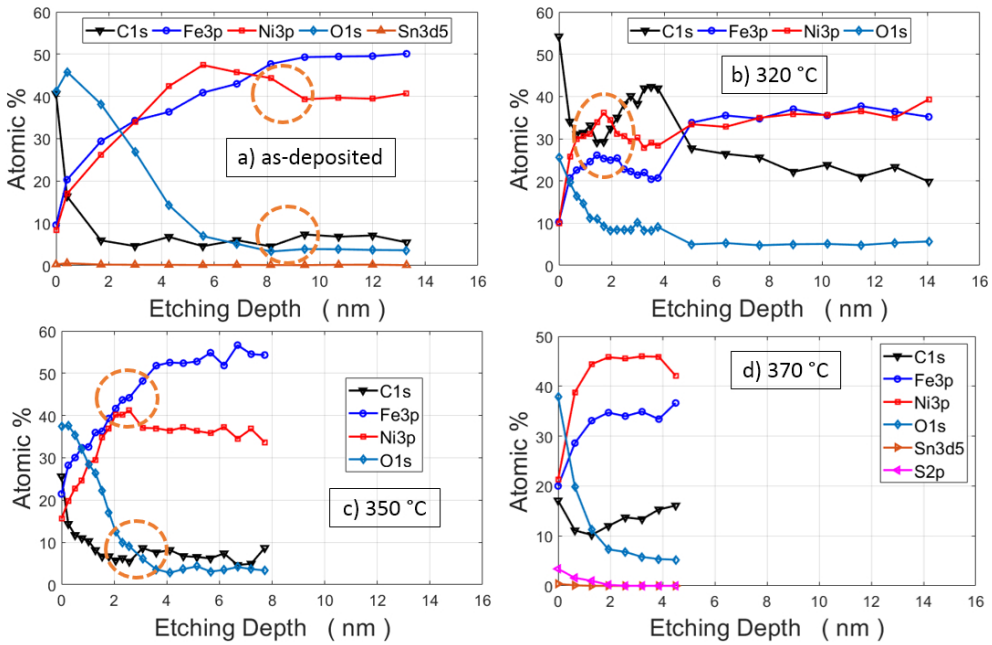

Figure 4: XPS quantitative depth profile of the top view surface: a) as-deposited sample; annealed samples at b) 320 °C, c) 350 °C and d) 370 °C. The dashed circles denote local drop in C opposed to an increase in Ni or vice versa.

278x180mm (100 x 100 DPI)

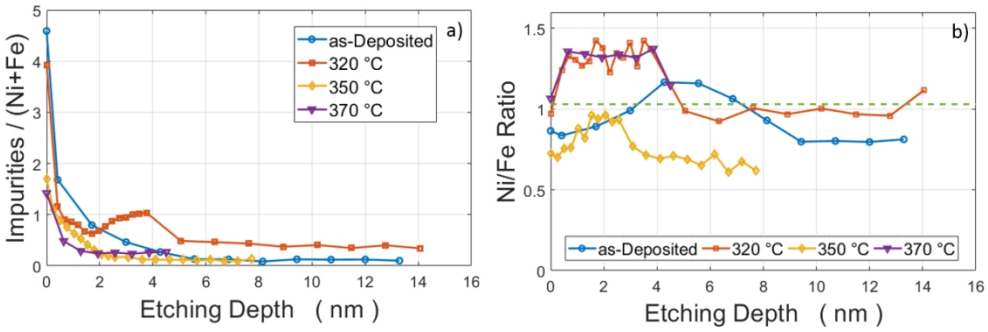

Figure 5: Comparison of XPS results between Ni-49 at%Fe alloy as-deposited and annealed samples at 320 °C, 350 °C and 370 °C conditions in terms of a) impurity/(Ni+Fe) ratio vs. etching depth and b) Ni/Fe atomic ratio vs. etching depth; the dashed horizontal line represents the nominal Ni/Fe ratio.

109x37mm (300 x 300 DPI)

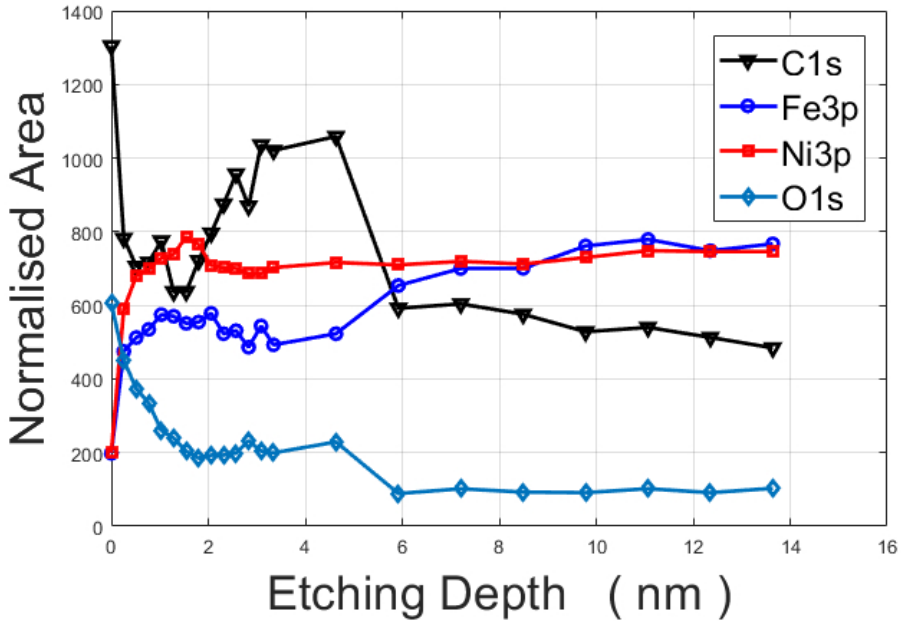

Figure 6: XPS normalised area vs. etching depth of the top view surface of the annealed sample at 320 °C; the dashed circles inscribes the region of local decrease in C opposed to an increase in Ni

184x121mm (96 x 96 DPI)